Context-Informed Conditional Anomaly Detection Approach for Wave Power Plants: The Case of Air Turbines

Jose Ignacio Aizpurua[1,3*], Markel Penalba [2,3], Natalia Kirillova [1], Jon Lekube [4], Dorleta Marina [4, 5]

[1]*Signal Theory & Communications Department, Mondragon University, Goiru 2, 20500 Arrasate, Spain*

[2]*Fluid Mechanics Department, Mondragon University, Loramendi 4, 20500 Arrasate, Spain*

[3]*Ikerbasque, Basque Foundation for Science, Euskadi Plaza 5, Bilbao, Spain*

[4]*Renewable Energy and Resource Usage Area, Basque Energy Agency, Urkixo Zumarkalea 36, 48011 Bilbao, Spain*

[5]*Biscay Marine Energy Platform, Atalaia 2 Bajo, Armintza 48620, Spain*

Abstract

The reliability and energy production of wave power plants (WPPs) depend on sea-state conditions, operation efficiency and degradation of its constituent assets. Air turbines are key assets for the efficient and reliable operation of WPPs and ensuring their correct operation leads to enhance the efficiency of WPPs. However, the lack of run-to-failure data and scarce fault records hampers the development of predictive condition monitoring solutions. In this context, focusing on unsupervised health monitoring methods, this paper presents an air turbine conditional anomaly detection (CAD) approach with a practical case study tested and validated on the Mutriku wave power plant. In contrast to anomaly detection models, which model the health-state without taking into account the influence of the operating context, the proposed CAD approach learns the expected air turbine operation conditioned on specific sea-states information modelled through wave energy flux concepts. This is achieved through an ensemble of Gaussian Mixture models and the expectation-maximization algorithm. Results show that, the integration of sea-states in the anomaly detection learning process improves the discrimination capability of the CAD model compared with the anomaly detection model without sea-state information, reducing false positive events and improving the accuracy of the CAD model.

Keywords: **Marine Renewable Energy Monitoring, Anomaly Detection, Prognostics and Health Management, Turbine, Power Curve and Monitoring.**

*Corresponding author

Email addresses: jiaizpurua@mondragon.edu (Jose Ignacio Aizpurua[1,3]), mpenalba@mondragon.edu (Markel Penalba [2,3]), nkirillova@mondragon.edu (Natalia Kirillova [1]), jlekube@eve.eus (Jon Lekube [4]), dmarina@bimep.eus (Dorleta Marina [4, 5])

1. Introduction

The ocean environment hampers the commercial viability of Marine Renewable Energy (MRE) technologies owing to the complexity to conceive balanced designs with the capacity to maximise energy harnessing and survivability, without excessive over-engineering. The harsh ocean environment accelerates the degradation of the different components of MRE devices and maintenance operations for offshore plants are significantly more complex and costly due to the limited accessibility, and the highly specialised vessel and crew requirements. Therefore, condition monitoring of MRE technologies is crucial because apart from the high maintenance cost, no energy is generated during longer downtimes.

In fact, production losses due to unavailability can result in downtime losses of up to 24 k€/MW (12 M€/year for a 500 MW offshore wind farm) Rinaldi et al. (2021b). As a consequence, operation and maintenance (O&M) costs associated with an offshore farm are estimated to be approximately 30% of the total income (for a 20-year lifetime), as opposed to 10-15% O&M costs associated with onshore farms Sorensen & Sorensen (2012).

However, due to the vast energy resource available in the ocean and more appealing characteristics of this resource, *e.g.* predictability and consistency, MRE systems are foreseen to be a key resource in the short- and long-term roadmaps towards a carbon-neutral energy system European Commision Communication (2020, 2019). The annual energy generation potential for offshore wind and wave is estimated in 420,000TWh IEA (2019) and 29,500TWh Mørk et al. (2010), respectively, representing together 19.5 times the current global electricity demand approximately.

Therefore, in order to make MRE technologies commercially viable, the development of intelligent and efficient O&M strategies is vital. These strategies should include, at least, the following four aspects:

1. Prediction of resource characteristics to assess plant accessibility.
2. Evaluation of MRE plant availability updated with condition-monitoring models.
3. Prediction of energy generation capabilities of the MRE plant.
4. Assessment of downtime and O&M costs.

The literature shows studies on some of these aspects, especially focusing on the more mature offshore wind industry. The accessibility of offshore wind farms is covered by Guanche et al. (2016), where a methodology to assess the accessibility to a floating wind turbine is evaluated concluding that the accessibility-limiting wave height threshold is highly dependent on wave direction and peak period. More recently, Gilbert et al. (2021) suggests a novel probabilistic method focused on forecasting safety-critical accessibility conditions.

Similarly, several condition monitoring approaches for offshore wind turbines components are present in the literature, such as turbine blades Martinez-Luengo et al. (2016), power transmission systems Feng et al. (2013), electric generators Vedreño-Santos et al. (2014) and power electronic components Jlassi et al. (2015). In addition to the component-level solutions, system-level methods have been also developed analysing component interactions and their impact on the system Santos et al. (2015). Overall, Mérigaud & Ringwood (2016) provides a comprehensive review of different methodologies and applications.

The prediction of energy generation capabilities have also been widely covered in the literature for different MRE technologies. Based on the wave climate of a specific location, the energy generation capabilities have been predicted using the capacity factor of the device/plant for longer periods Yue et al. (2019), power curves Gupta & Nem (2016) methods, or more sophisticated dynamic models that are usually suggested for floating offshore wind turbines (FOWTs) Cottura et al. (2021).

The economical evaluation of downtime and O&M services is also widely covered for wind turbines, including offshore wind turbines. A common metric of the economic aspects is the Levelised Cost of Energy (LCoE), which has been analysed in the literature for fixed offshore wind turbines Ioannou et al. (2018) and FOWTs Martinez & Iglesias (2022). In fact, Rinaldi et al. (2021a) incorporated the O&M models into the techno-economic analysis of FOWTs.

While some of the methodologies suggested for offshore wind have a direct application on the wave energy sector, *e.g.* accessibility models and part of the cost analysis, differences in the energy harnessing process makes necessary to develop novel methods. Energy generation prediction models, for example, are widely covered for different devices, with a wide variety of modelling techniques and complexities Penalba & Ringwood (2016). However, mainly due to the immaturity of the wave energy sector, prognostics and health management (PHM) solutions are scarce. In fact, operational data covering relatively long periods of time is often used for the different PHM studies, which does not exist in the case of wave energy. This data can also be replaced with run-to-failure data generated in laboratory environment through accelerated ageing tests, but these datasets are very limited to the best of authors' knowledge.

One of the very few exceptions worldwide is the Mutriku Wave Power Plant (WPP), further described later in Section 4. The Mutriku WPP is a wave energy conversion plant based on the oscillating water column (OWC) technology commissioned by the Basque Energy Agency in 2011 Torre-Enciso et al. (2009). It is one of the pioneer grid-connected WPPs worldwide. It has been operating for the last 10 years, reporting different degradation and failure events for different components. Due to the easily accessible location of the WPP, maintenance operations are not the most critical aspect. However, the generated data is highly valuable to develop PHM applications that will be vital for the reliable operation of future WPPs located far from shore.

The authors intentionally focus on the anomaly detection problem, motivated by the lack of run-to-failure data and scarce fault records. The operation of WPPs is highly variable, as is the ocean resource, and accordingly, the anomaly detection problem becomes a challenging task. Usually, anomalies are identified by comparing the plant operation against pre-defined normal behaviour. When a variable differs from what is expected under normal operating conditions, it may flag an anomaly. However, when the normal behaviour is highly-variable, the definition of conditions that represents the normal behaviour is a challenging task. Therefore, an accurate anomaly detection technique for WPPs requires information about the operation context to reduce false positives.

In fact, to the best of authors' knowledge, such a context-informed anomaly detection framework for WPPs has never been suggested in the literature. Hence, this paper presents a novel conditional anomaly detection approach focused on air turbines operated in OWC devices, where the context information is represented by sea-state conditions. The approach has been tested in the Mutriku WPP and results show that the integration of environmental sea-state information along with WPP parameters in the anomaly detection learning process, improves the discrimination capability of the CAD model compared with the anomaly detection model without sea-state information, reducing false positive events and improving the accuracy of the conditional anomaly detection model.

The remainder of this paper is organised as follows. Section 2 presents the integrated PHM framework for WPPs and reviews more specific state-of-the-art for anomaly detection problems. Section 3 presents the conditional anomaly detection model developed within the PHM framework. Section 4 presents the Mutriku WPP case study and Section 5 shows results by applying the developed approach to the case study. Section 6 discusses the proposed approach and Section 7 draws conclusions.

2. PHM framework for Wave Power Plants

Figure 1 shows the block diagram of the integrated PHM framework for a generic WPP. The framework combines expert knowledge of plant engineers with collected data to detect anomalies, diagnose failure causes, and predict the remaining useful life (RUL) of plant components Aizpurua & Catterson (2015).

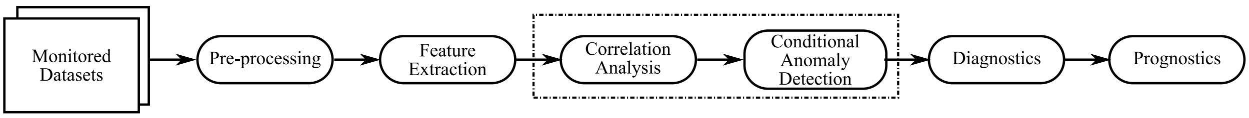

Figure 1: PHM framework for a generic WPP, highlighting the focus of this work.

Monitored variables of the WPP are firstly processed to discard missing and invalid values and filter noisy signals. Then pre-processed datasets are used to extract features that represent plant health information in different statistical, temporal and frequency domains. After the feature extraction step, the correlation analysis informs about dependencies between variables. These dependencies can be post-processed to develop different applications, such as the identification of deviations from normal operation conditions through changes in dependencies.

Anomaly detection models focus on the identification of deviations from expected normal operation conditions. They can be useful to define alarm systems or trigger further predictive analysis activities and react to the observed condition. Diagnostics models focus on the identification of the actual health state Vachtsevanos et al. (2006). This classification can be based on predefined groups of health states or it can be centred on the estimation of the actual health state through *e.g.* filtering strategies Aizpurua et al. (2020). Prognostics models focus on the prediction of future degradation trajectories and RUL estimation based on likely life-stressors and operational profiles Aizpurua et al. (2019). This research focuses on the development of an adequate anomaly detection approach and development of diagnostics and prognostics models within the PHM framework are left for future work (cf. Section 7).

There exist limited monitoring solutions for marine energy applications, such as tidal turbine degradation modelling Galloway et al. (2017), or wave energy converter health monitoring through underwater acoustic emission Walsh et al. (2017). The development of monitoring solutions for tidal turbines and wave energy applications based on power curve modelling is a challenging approach, because it is necessary to model the sea-state information and evaluate its influence on the generated power Mérigaud & Ringwood (2016). Technological solutions for wind energy have been developed for many years now and, accordingly, most of the proposed turbine condition monitoring solutions focus on wind turbines de Novaes Pires Leite et al. (2018). Technological similarities between air-turbines implemented in OWC devices and wind turbines suggest that methodologies applied on wind turbines may be applicable to air-turbines.

Wind turbine anomaly detection approaches can be classified into data-driven and model-based approaches Hameed et al. (2009); Kusiak et al. (2013). Model-based methods develop physics-based operational models and data-driven methods define the expected operation through operational data measured via supervisory control and data acquisition (SCADA) systems. Anomaly detection models for wind turbines have often been addressed in the literature through probabilistic power curve models using statistical learning models, such as copulas Gill et al. (2012) and Gaussian processes Pandit & Infield (2018).

In other engineering contexts, different unsupervised anomaly detection approaches have been proposed. Vanem & Brandsæter (2021) evaluate different unsupervised anomaly detection methods tested on marine diesel engine data, including Self-Organising Maps (SOM), k Nearest-Neighbor (kNN), density-based clustering (DBscan), Gaussian Mixture Models (GMM) and one-class Support Vector Machines (SVM). They provide an insightful discussion about the hyper-parameter selection, relevance of training data and the effect of dimensionality reduction. Coraddu et al. (2019) develop two anomaly detection models using kNN and SVM models to monitor hull and propeller performance. These unsupervised anomaly detection models, evaluate the available dataset to explore anomalies without ground truth information. In Vanem & Brandsæter (2021) different models are tested and it is possible to validate results by checking the consistency across models. In Coraddu et al. (2019) labels are used to evaluate the performance of the anomaly detection models.

In a similar direction, Baraldi et al. (2015) presented an application of the Auto-Associative Kernel Regression (AAKR) approach Hines & Garvey (2006), which focuses on fitting normal data to a AAKR model, subsequent signal reconstruction and comparison with monitored parameters. The performance of the approach is dependent on the learned signal properties and it has been enhanced in Brandsæter et al. (2019) for large datasets including memory vectors modelled as clusters. So as to enhance the learning abilities of anomaly detection models, autoencoder (AE) architectures were proposed building representations of the original signal encoded in deep Artificial Neural Network layers, and then evaluate reconstructions of monitored signals with the designed AE model, which can integrate signal properties in the different neurons and layers of the AE model Wu et al. (2020). AAKR and AE models, perform adequately in controlled environments and they have shown an excellent ability to learn independent signal properties over time. However, they lack of contextual information.

Anomaly detection without contextual information is a challenging task, which can create spurious jumps in the data and penalize the performance of the anomaly detection model Vanem & Brandsæter (2021). In this direction, so as to cover the range of operation and reduce false positives, ensemble strategies have been proposed by combining multiple anomaly detection models, such as the ensemble of hidden Markov models combined through kappa measurements to reach diversity and detect multiple anomalies Islam et al. (2018). Recently, transfer learning concepts have been also implemented to complement operational data with different operation conditions through adversarial deep-learning concepts Michau & Fink (2021).

It can be observed that existing anomaly detection models perform appropriately under stable operation conditions, but show a poor performance without contextual information. This can be partially handled with an ensemble of anomaly detection models, but it is necessary to design multiple and diverse models that can capture characteristics of different operation conditions. The operation and degradation of WPP is strongly influenced by metocean conditions Mérigaud & Ringwood (2016), and in such cases, it is necessary to incorporate sea-state information in the modelling process. One possibility to achieve this objective is the adoption of conditional anomaly detection (CAD) modelling concepts Song et al. (2007), where the main goal is to learn and model the normal operation condition of the system as a function of the operation context. Catterson et al. (2010) presented a conditional anomaly detection model for transformer monitoring taking into account environmental parameters such as meteorological conditions and applied electrical load, along with transformer condition data such as oil temperature and dissolved gasses.

However, to the best of authors' knowledge, contextual anomaly detection concepts have not been developed for wave power plants and this is the original contribution of this paper. The proposed approach makes use of unsupervised machine learning methods so as to model air turbine operation states, which are statistically correlated with contextual sea-state information to learn likely normal operation states along with associated sea-state conditions. The approach is tested and validated with real data collected in the Mutriku WPP, including fault events that are used to validate the proposed model.

3. Air-Turbine Conditional Anomaly Detection Approach

The main focus of this paper is on the development of a CAD model for air turbines operated in WPPs. The implementation of this approach will permit the prompt detection of anomalies while avoiding false positives and unplanned maintenance actions.

The expected operation of an air turbine can be modelled using the characteristic power curve, which relates the rotation speed with the produced power. Figure 2 shows the power curve of the turbine T10 of the Mutriku WPP using the monitored SCADA data corresponding to 10/09/2019-10/12/2019. It can be observed that the saturation point is located near 3200 rpm with an approximated maximum produced power of 22 kW. Negative power values indicate that the WPP absorbs energy from the grid to prevent the turbine from stopping.

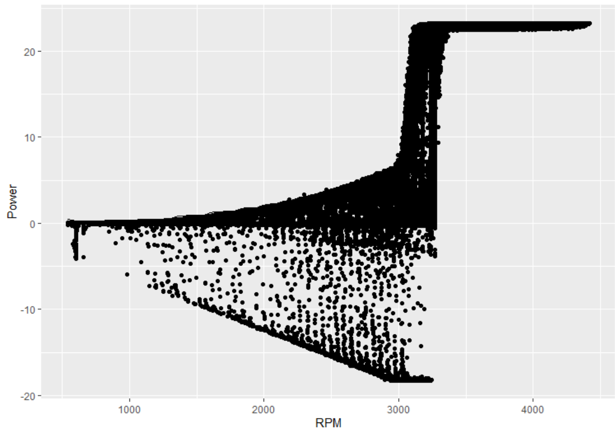

Figure 2: Mutriku WPP power curve.

Deviations from the characteristic power curve may indicate early warnings or abnormal turbine operation states Gill et al. (2012). However, the operation of air turbines is surrounded by different sources of uncertainty, such as stochastic sea-state and atmospheric conditions, and accordingly, it is necessary to capture uncertainty modelling criteria along with the power curve.

In the context of anomaly detection models, it is crucial to reduce false positives and maximize accuracy. Different operation conditions may result in different performance indicators, and therefore, it is very important to learn the normal behaviour of the turbine with respect to its operation context.

Accordingly, this paper defines a framework to jointly model expected turbine performance conditions along with the corresponding expected sea-state. Figure 3 shows the developed conditional anomaly detection model for the air turbine, where turbine operation data is combined with environmental conditions and the operation of the turbine is evaluated conditioned to the environmental information.

The environmental model will be determined through the combination of significant wave height H_s and the peak period T_p, which are common statistical parameters to characterize a sea-state Ardhuin et al. (2019). Subsequently, probabilistic multivariate models will be developed for the turbines to characterize the corresponding probabilistic power curve of the turbine. Finally, their probabilistic correlations will be defined so as to estimate the probability of a turbine being healthy, given the operational information.

3.1. Environmental sea-state model

The environmental model will be defined through the wave energy flux (WEF), which models the energetic sea-state, and it is defined as follows:

$$WEF = 0.49\ H_s^2\ T_e, \tag{1}$$

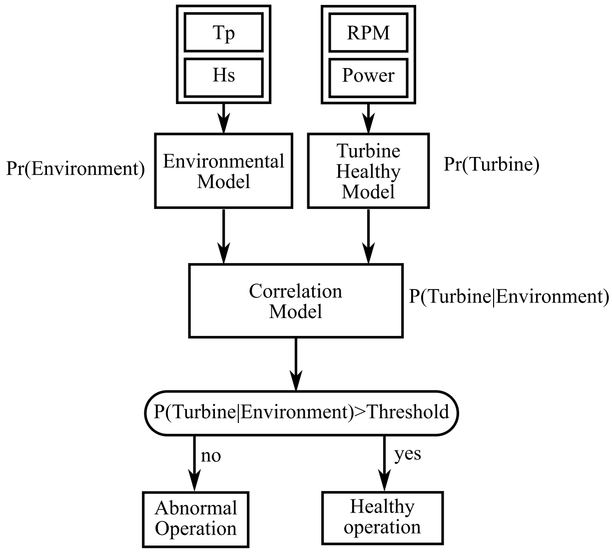

Figure 3: CAD framework for air turbines.

where T_e is the energetic period defined as follows:

$$T_e = \alpha \; T_p \tag{2}$$

where $\alpha = 0.9$ is considered as suggested in Tucker & Pitt (2001).

It is expected that higher energetic sea-states, that are characterized with high WEF values, will operate with a different power curve compared with low energetic sea-states. Accordingly, the expected operation conditions, including the rotational speed and generated power, will be different depending on the sea-state.

In this paper, different sea-states have been organized into different levels according to their energy flux values (see Section 4). The classification criteria is solely based on expert-knowledge and the use of data-driven clustering strategies is left for future work.

3.2. Air Turbine model

The power curve of the air turbine model will be developed using multivariate probabilistic distributions through Gaussian Mixture Models (GMM) Song et al. (2007). GMMs can model multivariate distributions and they enable capturing uncertainties through mixture of Gaussian distributions.

For each power curve sample, comprised of the pair $x_i = \{r_i, e_i\}$, where r denotes the rotational speed of the generator (in rpm units), and e denotes the generated energy (in kW units), the PDF of the GMM, $f_{GMM}(x_i)$, is defined through a set of Gaussian distributions $k \in \{1, \ldots, K\}$ mixed in different proportions:

$$f_{GMM}(x_i|\mathbf{\Theta}) = \sum_{k=1}^{K} \alpha_k P(x_i|\theta_k) \tag{3}$$

where $\{\alpha_1,\ldots,\alpha_K\}$ are the mixing probabilities, each θ_k is the set of parameters defining the k-th component, and $\mathbf{\Theta}$ is the complete set of parameters needed to specify the mixture, $\mathbf{\Theta} \equiv \{\theta_1, \ldots, \theta_K, \alpha_1, \ldots, \alpha_K\}$.

In the univariate case, the likelihood of new measurements x_i given the GMM parameters, $P(x_i|\theta_k)$, is defined as follows:

$$P(x_i|\theta_k) = \frac{1}{\sigma_k(\sqrt{2\pi})} exp(-\frac{1}{2}\frac{(x-\mu_k)^2}{\sigma_k^2}) \tag{4}$$

where σ_k^2 is the variance and $\theta_k = \{\mu_k, \sigma_k\}$.

Eqs. (3) and (4) define the GMM model for the univariate case. They are extended for the multi-dimensional case by defining the likelihood function as follows:

$$P(x_i|\theta_k) = \frac{1}{(2\pi^d \det|\mathbf{\Sigma}_k|)^{\frac{1}{2}}} exp(-\frac{1}{2}(x_i - \boldsymbol{\mu}_k)^T \mathbf{\Sigma_{\boldsymbol{k}}}^{-1}(x_i - \boldsymbol{\mu}_k)) \tag{5}$$

where d is the dimension of the data, $\boldsymbol{\mu}_k$ is the mean vector, $\mathbf{\Sigma}_k$ is the covariance matrix, and $\theta_k = \{\boldsymbol{\mu}_k, \mathbf{\Sigma}_k\}$.

Given a set of n data samples, $\mathbf{X} = \{x_1 \ldots, x_n\}$, the log-likelihood corresponding to a k-th component mixture is:

$$log(P(\mathbf{X}|\mathbf{\Theta})) = log \prod_{i=1}^{n} P(x_i|\mathbf{\Theta}) = \sum_{i=1}^{n} log \sum_{k=1}^{K} \alpha_k P(x_i|\theta_k) \tag{6}$$

The direct maximization of the log-likelihood function in Eq. (6) is complex and cannot be found analytically. Usually the maximum likelihood estimation is obtained using the expectation-maximization (EM) algorithm Song et al. (2007), which learns the distribution parameters $\boldsymbol{\theta}$ from the data, and this is the algorithm implemented in this research for the inference of the distribution parameters.

In general, GMMs represent the probability distributions of the given observations. Learned GMM distributions can be used to make statistical inferences about the properties of the given observations. In an unsupervised clustering context, GMM modelling focuses on grouping data based on a mixture of, possibly multivariate, Gaussian distributions. This leads to construct clusters which are ellipsoidal, centred at the mean vector, and with varying geometric features such as volume, shape and orientation determined by the covariance matrix $\mathbf{\Sigma_{\boldsymbol{k}}}$. It is possible to parametrize the covariance matrix through the eigen-decomposition, which leads to the following definition Celeux & Govaert (1995):

$$\mathbf{\Sigma_{\boldsymbol{k}}} = \lambda_k D_k A_k D_k^T \tag{7}$$

where λ_k is a scalar controlling the volume of the ellipsoid, A_k is a diagonal matrix specifying the shape of the density contours with $det(A_k)$=1, and D_k is a diagonal matrix which determines the orientation of the corresponding ellipsoid.

The volume, shape and orientation of the covariances can be constrained to be equal or variable across different groups which leads to the definition of different clusters with different characteristics and shapes as defined in Table 1 and implemented in the `mclust` package Scrucca et al. (2016).

Table 1: Parametrisation of the covariance matrix $\boldsymbol{\Sigma_k}$ for multidimensional data Scrucca et al. (2016).

Model	$\boldsymbol{\Sigma_k}$	***Distribution***	***Volume***	***Shape***	***Orientation***
EEI	λI	Spherical	Equal	Equal	-
VII	λ_kI	Spherical	Variable	Equal	-
EEI	λA	Diagonal	Equal	Equal	Coordinate axes
VEI	λ_kA	Diagonal	Variable	Equal	Coordinate axes
EVI	λA_k	Diagonal	Equal	Variable	Coordinate axes
VVI	$\lambda_k A_k$	Diagonal	Variable	Variable	Coordinate axes
EEE	λDAD^T	Ellipsoidal	Equal	Equal	Equal
EVE	λDA_kD^T	Ellipsoidal	Equal	Variable	Equal
VEE	$\lambda_k DAD^T$	Ellipsoidal	Variable	Equal	Equal
VVE	$\lambda_k DA_kD^T$	Ellipsoidal	Variable	Variable	Equal
EEV	$\lambda D_kAD_k^T$	Ellipsoidal	Equal	Equal	Variable
VEV	$\lambda_k D_kAD_k^T$	Ellipsoidal	Variable	Equal	Variable
EVV	$\lambda D_kA_kD_k^T$	Ellipsoidal	Equal	Variable	Variable
VVV	$\lambda_k D_kA_kD_k^T$	Ellipsoidal	Variable	Variable	Variable

The selection of the optimal model, *i.e.* number of Gaussian components and the covariance parametrization that minimise error, is selected by maximizing the Bayesian Information Criterion (BIC). The BIC is a penalized form of log-likelihood. That is, the log-likelihood increases with more components and a penalty term is subtracted to compensate for this event. The BIC is defined as follows:

$$BIC_{M,G} = 2log(L_{M,G}) - mlog(n) \tag{8}$$

where $log(L_{M,G})$ is the maximized log-likelihood for the model M with G components, m is the number of estimated parameters in the model, and n is the number of observations in the data. The pair $\{M, G\}$ which maximizes the $BIC_{M,G}$ is selected as the optimal model.

Note that the BIC definition in Eq. (8) may be defined as a minimization problem if the negative log-likelihood and positive penalization term is used. The BIC criteria has been used because it shows a good compromise between model complexity and accuracy, as compared with other information criterion metrics such as Akaike information criteria. Penalized forms of BIC, such as the integrated complete likelihood (ICL), which penalizes BIC through an entropy term, shows the same performance and model-selection, as also observed in Vanem & Brandsæter (2021), and accordingly, the simpler BIC definition has been used. ICL seems to be a preferred solution for unsupervised problems with well-separated clusters Scrucca et al. (2016).

3.3. Correlation Model

The correlation between the environment model and the turbine model is determined by the classification of sea-states into different groups and associating the corresponding power curve to each group. Figure 4 shows the conceptual diagram of the conditional anomaly detection model, where the $Pr(Environment)$ block shows a random classification of the different sea-states.

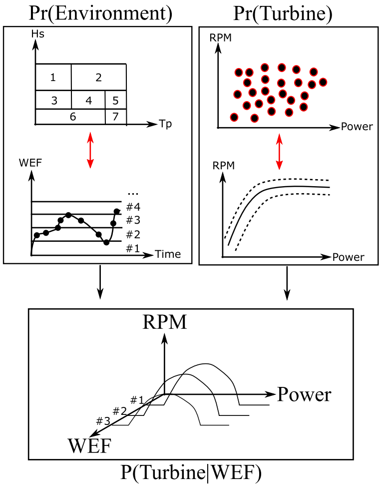

Figure 4: CAD for air turbines operated in the WPP.

The environmental model in Figure 4 shows the discretization of the pair $\langle H_s, T_p \rangle$ into the corresponding WEF sea-state level and characterization of the corresponding power curve.

The empirical power curve will be conditioned on the sea-state classification criteria, $Pr(Turbine|\text{WEF})$, and it will be constructed accordingly. Figure 5 shows this concept by defining three states, with predefined WEF values to classify signals into one of these states.

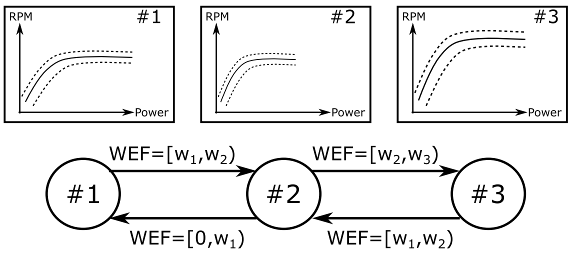

Figure 5: WEF states and corresponding power curve.

The transition conditions between different sea-states are deterministic boundary WEF values. The extension of the framework to include probabilistic transition rates is left for future work.

4. Case Study

The approach suggested in Section 3 is tested on the Mutriku WPP located in the Gulf of Biscay. The WPP is constructed onshore, integrated into a breakwater that protects

Mutriku's fishing harbour, as shown in Figure 6 (a). The WPP is based on the OWC principle and consists of 16 independent air chambers with their corresponding air-turbine and electric generator, as illustrated in Figure 6 (b). The OWC technology uses wave energy to pressurize air in a chamber forcing it through an air turbine. The incoming and outgoing movement of the sea water within the chamber creates a bidirectional air flow through the turbine. In turn, the turbine is coupled to a power generator which produces energy.

Due to the bi-directional reciprocating air flows generated in the air chambers of OWC devices, self-rectifying turbines are designed specifically for this application. A number of self-rectifying turbines have been suggested in the literature Falcao & Gato (2012), being the Wells turbine the most popular and the one installed in the Mutriku WPP.

The 16 air chambers of the Mutriku WPP are equipped with a set of Wells turbines and an electric generator of 18.5 kW rated power. However, the maximum allowed power of the generator is extended until 22.5 kW in order to maximise the energy harnessing capabilities of the WPP. It should be noted that the first and last chambers are disabled and, thus, only 14 out of 16 chambers are currently operational, resulting in a total rated power of 260 kW (instead of the total capacity of 296 kW) Fäy et al. (2020). In addition to the turbine-generator set, Figure 6 (b) shows the turbine chamber. Currently, the Biscay Marine Energy Platform (BIMEP) is the responsible for the operation and maintenance tasks of the plant.

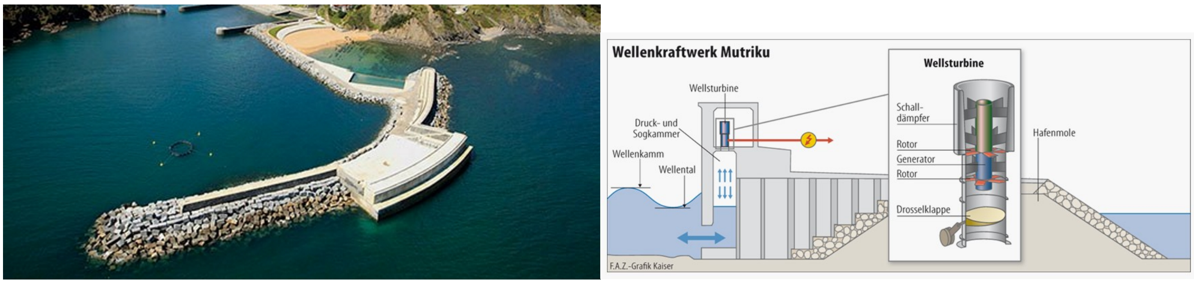

(a) Panoramic view. (b) OWC chamber and turbine.

Figure 6: Mutriku WPP.

From the beginning of the operation of the Mutriku WPP, different degradation and failure events have been reported for WPP components including air-turbines and electric generators Lekube et al. (2018), which required unplanned maintenance actions. The lack of experience in similar systems hampered the development of condition monitoring strategies, and maintenance actions have been adopted through intuition and expert knowledge.

Although grid-connected, the main goal of the Mutriku WPP is promoting the development of OWC components, auxiliary systems and control strategies. Therefore, the operational consequence of unplanned maintenance actions are not as critical as in future commercial open ocean WPPs. However, the monitored information of the plant operation can be used to develop health monitoring models that integrate statistical learning strategies with expert knowledge, and accordingly, assist engineers in the maintenance decision-making processes of future WPPs. Since the CAD approach suggested includes monitored data from the environment and the WPP, each datasets are described in the following subsections.

4.1. Turbine Operational Data

The WPP operates in different modes, automatically identifying the operation mode for each turbine depending of the operation characteristics. In a simplified manner, the WPP starts the operation from shutdown with a *start-up* mode, jumping to *power production* mode once the start-up is completed. Under normal operation, the WPP remains in *power production* mode passing through *self-check* mode automatically every 24 hours to verify the correct operation. If the plant is operating at low power or high pressure levels, the WPP enters in *low-power inhibit* or *high-power inhibit* modes, respectively, returning back to *power production* mode when the pressure in the chamber increases in the former case and decreases in the latter. In the case of a serious fault or any other suspicious event, the WPP can be shut down manually so that maintenance operations can be carried out safely. The SCADA system implemented in the Mutriku WPP includes a flag that records the plant operation mode at each instant.

The main objective of the developed CAD approach is to identify anomalies that go unnoticed for the described high-level semi-automatic operating system. The *power production* mode is the most relevant operation because it is the energy generation mode, and accordingly, the operation data for this mode is isolated from the rest.

For this operation mode, turbines in the Mutriku WPP are controlled combining maximal torque control and flux weakening strategies as shown by Fäy et al. (2020). Maximal torque control is applied when the turbine rotates below the nominal rotational speed, while the flux-weakening strategy comes into play above the nominal rotational speed. Due to this control combination, turbines may operate over its nominal power for a short period of time (up to the previously mentioned 22.5 kW maximum allowed limit). Therefore, the behaviour of the turbines is also conditioned by the control law applied in the turbo-generator, as shown by several studies for different turbines in the context of the Mutriku WPP, *e.g.* Lekube et al. (2016); Fäy et al. (2018); Otaola et al. (2019); Fäy et al. (2020). As a consequence, it can be assumed that control will have a significant role on the appearance of anomalies.

Hence, rotational speed is the variable that affects most in the generated power and, as a consequence, both variables are used in the CAD approach presented in this study. In addition, these two variables are the ones that show the highest correlation among all the monitored mechanical variables. In order to limit the scope of the study the turbine T10 in the Mutriku WPP is studied extracting data for the period 10/09/2019-10/12/2019. This period of time provided the most consistent set of data for the analysis. Figure 7 (a) shows the instantaneous measurements for rotational speed, power, pressure and vibrations from top to bottom, while the correlation among the different variables is shown in Figure 7 (b).

4.2. Environmental Data

For the context-informed CAD approach, the information about the context is provided by the sea-state conditions through the pair $\langle H_s, T_p \rangle$. These two statistical parameters can be combined for the computation of the WEF [cf. Eq. (1)], which provides the available wave power at a certain location per unit of wave-crest length. Although both T_p and H_s are vital for an accurate resource characterisation, the context information required by the

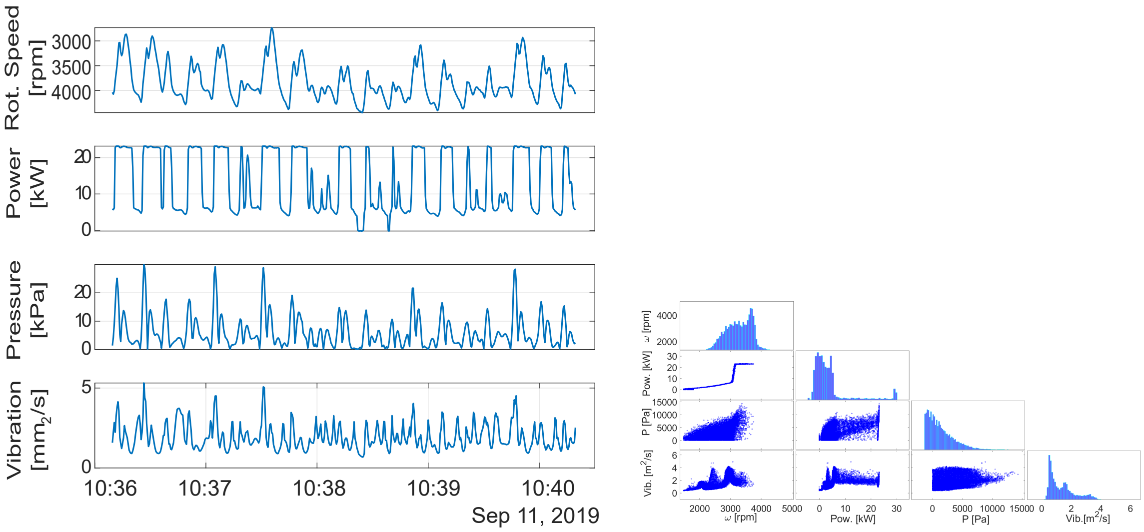

(a) Instantaneous measurements. (b) Correlation analysis of variables.

Figure 7: T10 air turbine monitoring.

CAD approach presented in this study must be synthesised in a single parameter, for which the WEF is selected.

Data on wave climate characteristics at a certain location can be obtained by means of two main sources: *in-situ* buoy measurements, *e.g.* Ruggiero et al. (2010) and Mérigaud & Ringwood (2018), and wave model and re-analysis datasets, *e.g.* Reguero et al. (2015) and Ulazia et al. (2020). *In-situ* buoy measurements are the most reliable source of data, which can provide direct measurements of the free-surface elevation or post-processed statistical parameters, such as T_p and H_s. The former requires a prohibitive on-board data storage capacity for a relatively small wave-riding buoy and, as a consequence, main oceanographic agencies provide mean statistical parameters of measured wave data.

However, *in-situ* data is not always available, due to geographical or temporal limitations. Wave model and reanalysis data are highly valuable in these cases, providing data that cover large geographical areas along various decades. In the present study, wave data from the SIMAR model is used. SIMAR is an ensemble of modelling metocean data created upon a high-resolution numerical model by the Spanish Oceanographic Agency Puertos del Estado, which covers the coast along the Iberian Peninsula between 1958-2020 with a temporal resolution of 1 hour. It is important, though, that in order to extract solid conclusions, model and reanalysis datasets should be adequately validated.

For this work, data from the SIMAR model in front of the Mutriku WPP is considered. Since no measurement data is available for this precise location, the validation of the SIMAR model data is carried out at the closest grid point of the SIMAR model for which *in-situ* data exists. Figure 8 (a) illustrates the geographical location for the Mutriku WPP, the Bilbao-Vizcaya (BV) measurement buoy of the Spanish Oceanographic Agency Puertos del Estado and the different grid points of the SIMAR model along the coast between the BV buoy and Mutriku WPP. The validation is recently carried out in Martinez-perurena et al.

(2021) between wave data at gridpoint 1 and *in-situ* measurements of the BV buoys and this validation of the SIMAR model is considered to provide confidence on the model in order to use the wave data that is closest to the Mutriku WPP at gridpoint 12 in Figure 8 (a). Figure 8 (b) shows the predominant wave direction in front of the Mutriku WPP.

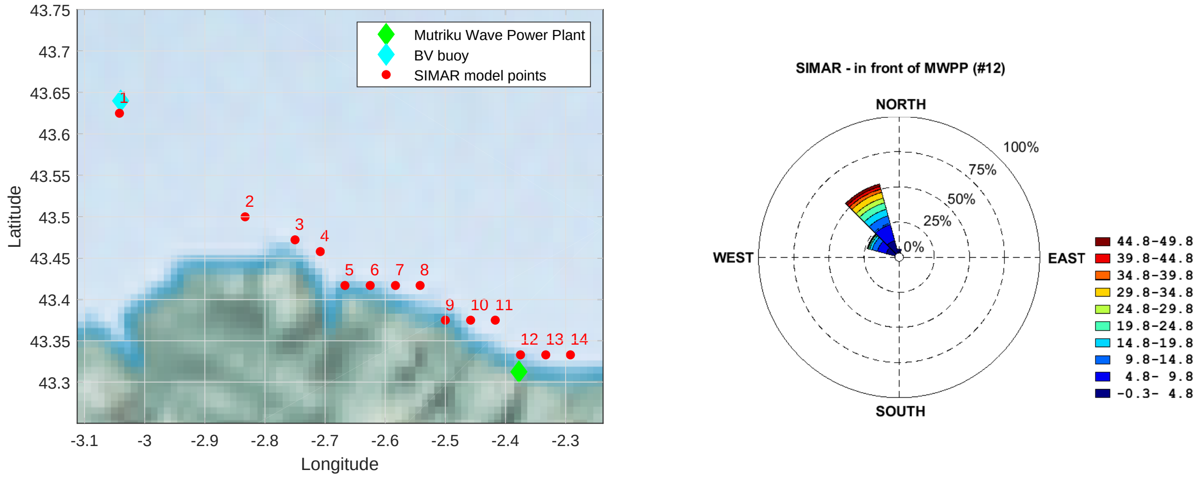

(a) Mutriku WPP, BV buoy, SIMAR gridpoints. (b) Predominant wave direction of the resource.

Figure 8: Wave resource data from the SIMAR model: (a) model gridpoint location, (b) wave rose.

So as to design a conditional anomaly detection model, the environmental data is categorised according to expert knowledge. Accordingly, the continuous WEF (with a temporal resolution of 1 hour) is discretised into five main groups. The discretisation criteria is based on the mean WEF at the Bay of Biscay, which is reported to be around 20 kW/m in different studies in the literature, *e.g.* Ulazia et al. (2017), resulting in five different categories as follows:

- WEF 1: Very low energetic sea-states: 0-5 kW/m
- WEF 2: Low energetic sea-states: 5-15 kW/m
- WEF 3: Medium energetic sea-states: 15-25 kW/m
- WEF 4: High energetic sea-states: 25-40 kW/m
- WEF 5: Very high energetic sea-states: 40+ kW/m

Figure 9 illustrates this discretisation comparing the continuous and discrete WEF signals for the period of time studied in this paper. As a consequence, as described in Figure 5, for each WEF configuration, the associated performance parameters of the WPP are monitored. Note that the mapping between sea-states and WPP health states is influenced by the propagation delay of sea-states that is jointly defined by the physical distance between the buoy and the WPP, and environmental conditions.

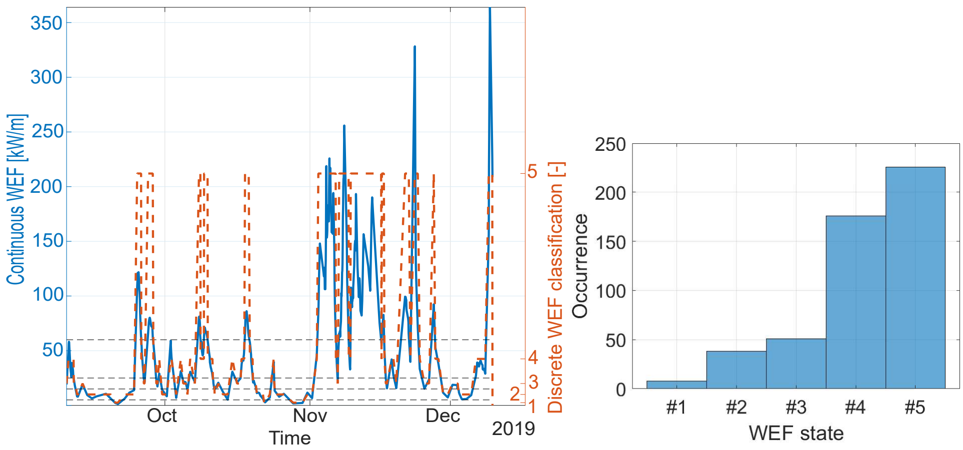

(a) Continuous vs. Discrete WEF. (b) Histogram of the WEF categories.

Figure 9: Wave energy flux based discretization of sea-states.

The selection of the number of sea-states impacts on the performance of the anomaly detection model. This is driven by engineering expert knowledge and leads to perform well in the tested scenario. However, changing the number of categories into less states, leads to obtaining a model which does not discern between different contextual information and causes false negatives. In contrast, increasing the number of states, leads to a very contextually-sensitive model, which flags false positive events.

5. Results

5.1. Data Pre-processing

Following the framework shown in Figure 3, the data preprocessing activity is comprised of three connected steps. Firstly, invalid data readings with abnormal values are removed so as to avoid biases in the data, such as out-of-range values and missing data. Subsequently, original 10 Hz sampled signals are downsampled into 5-minute averages, so as to avoid false positives with specific wave conditions and ensure the duration of anomalous events throughout the 5-minute intervals. Figure 10 shows the downsampled signals for generated power and rotational speed.

Finally, data-binning is implemented so as to ease the probabilistic analysis by converting data more suited for Gaussian components. Namely, the data-binning step counts as the same value data points differing by low values, and this step smooths the GMM learning process through the expectation-maximization algorithm avoiding the algorithm to collapse Song et al. (2007).

5.2. Correlation Analysis

In order to analyse the correlation between Mutriku WPP variables and sea-state information it is necessary to align both datasets. On the one hand, Mutriku WPP variables are collected through a SCADA system with a sampling rate of 10 Hz. On the other hand, the

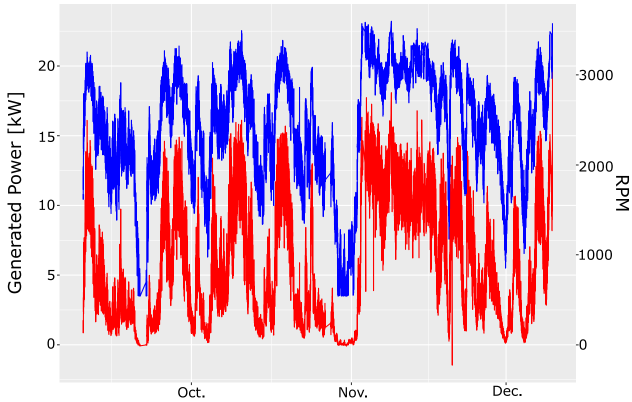

Figure 10: Pre-processed data from 10/09/2019 to 10/12/2019.

SIMAR model at the gridpoint #12 in front of the Mutriku WPP provides wave data with a temporal resolution of 1 hour. Figure 11 shows the evolution of the WEF (in blue) and the power generation of the Mutriku WPP (in red) for a 1-hour resolution.

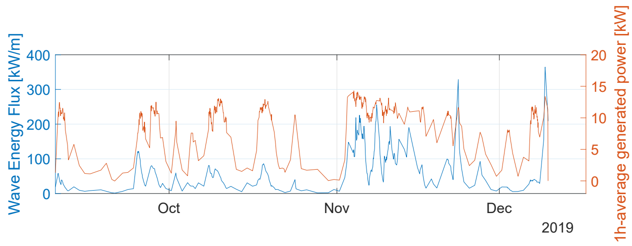

Figure 11: WEF and generated power.

In order to demonstrate the temporal alignment of wave resource and WPP datasets, a cross-correlation analysis is carried out comparing hourly wave data from the SIMAR model at the gridpoint #12 and the downsampled WPP variables with the same temporal resolution. The downsampling of the SCADA data to obtain hourly data is performed via time-integration of the generated energy within one-hour intervals. Figure 12 illustrates the cross-correlation analysis between the generated power and WEF, where no delay is shown. It should be noted that this delay is consistent across all the evaluated scenarios.

Finally, the correlation among the different WPP variables is studied in order to better understand the operation of the WPP. The Pearson correlation is low for all the variable pairs, meaning that the linear relationship between all variable pairs is low. However, non-linear relationships between some variable pairs are identified. The most relevant relationship is found between rotational speed and generated power. Figure 2 illustrates this relationship, where the saturation effect plays a significant role. In addition, negative power values appear for low-medium rotational speed ranges, which can be attributed to the control algorithm that prevents the turbine from stopping when wave power is low. Accordingly, the anomaly detection analysis in this study focuses on rotational speed and generated power so as to leverage the information of these variables for condition monitoring.

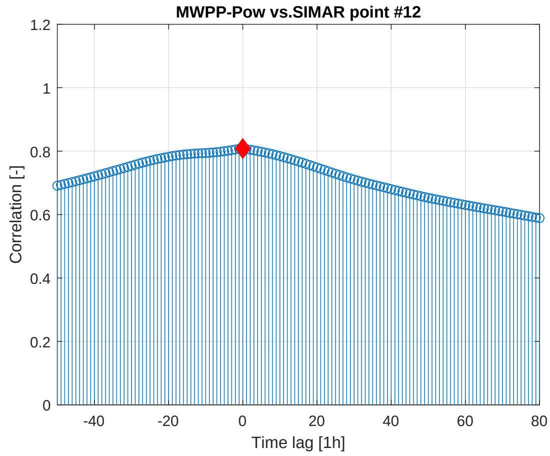

Figure 12: WPP-WEF cross-correlation for the WEF measured at BV buoy.

The same correlation analysis is also carried out for the five WEF categories and the corresponding rotational speed and generated power, as shown in Figure 13 (a). Despite the similarities of the different curves for all the WEF classes, the saturation effect of the generated power appears to be more significant as wave power increases.

5.3. Probabilistic models

Furthermore, a probabilistic descriptive operation analysis of the air turbines has been carried out in order to understand and characterize the expected operation of the air turbines as a function of sea-state conditions. Figure 13 (b) shows the different WEF groups and the associated distributions of the generated power corresponding to each group. It should be noted that the rated power of each generator is of 18.5 kW, but the plant operation allows power peaks up to 22.5 kW, which is the maximum allowed power (cf. Section 4.1).

It can be observed from Figure 13 (b) that:

- The overall distribution, including all the WEF classes, shows three main peaks located at (i) close to 0 kW, (ii) just above 5 kW and (iii) rated power 22.5 kW.
- The discrete, group-based WEF analysis highlights:
  - The WEF 1 distribution shows an unimodal distribution with the peak very close to 0 kW, illustrating a very low power generation.
  - WEF 2 is similar to WEF 1, but shows a wider and more positively-skewed distribution, indicating that power generation increases substantially. In addition, a tiny peak can be observed at the rated power of the turbine, meaning that the saturation effect has a subtle impact.
  - WEF 3 and WEF 4 show a very similar bimodal distribution with a broad peak at low power values and a significant narrow peak at the rated power value. Hence, the saturation effects is shown to have a relevant impact. The main difference is the higher relevance of the peak at the rated power in WEF 4.

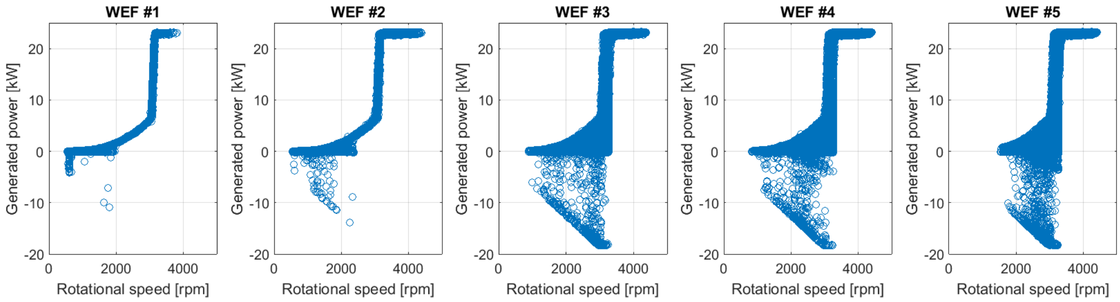

(a) WEF categories and associated power curves.

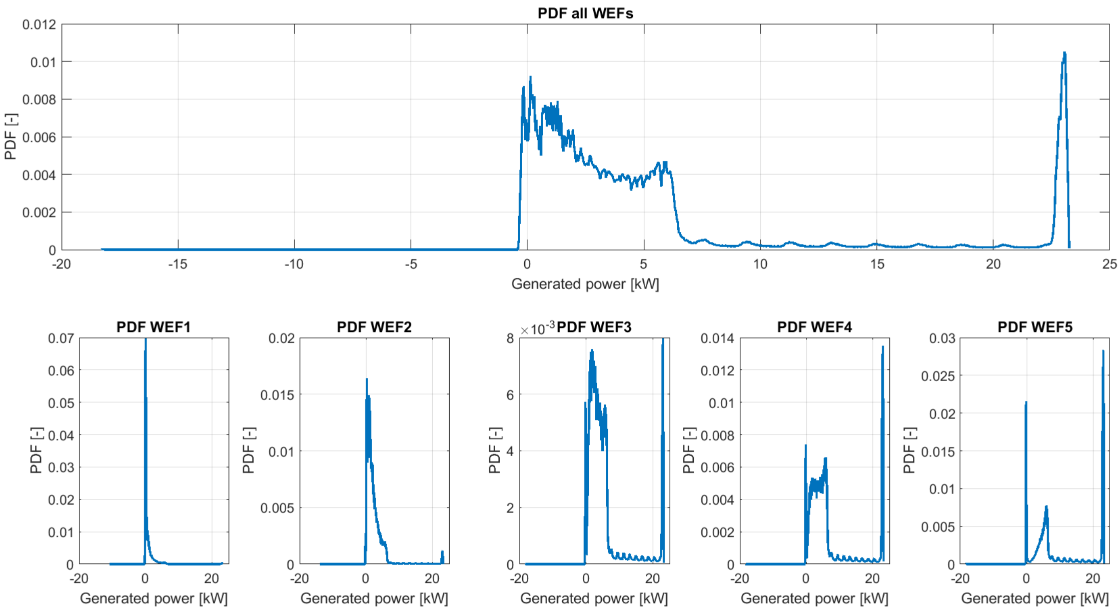

(b) WEF categories and associated distributions of WPP performance variables.

Figure 13: Mutriku WPP characterisation for each WEF class.

– Finally, WEF 5 shows a clear trimodal distribution with the three characteristic power generation values located at 0 kW, 5 kW and 22.5 kW.

5.4. Anomaly detection

In order to design the anomaly detection model of the air turbines, firstly, independent probabilistic operation models are designed fitted to different sea-state groups. The probabilistic operation models are based on empiric power curves that capture the dependency between the generated power and rotational speed. Figure 2 shows the empiric power curve of the WPP computed with the monitored dataset without separation into different sea-states.

From the available three months dataset, one month has been used to train the probabilistic models, and the subsequent two months have been used for testing the trained models. For the sake of manageability and in order to reduce false positives, available datasets are downsampled into 5-minutes averaged data. Averaging datasets reduces the otherwise prohibitive computational burden, smooths the monitored variables and removes instantaneous anomalous events. Note that wave data is also upsampled accordingly by means of a linear interpolation method.

Figures 14-18 shows the downsampled empiric power curves for the different WEF groups corresponding to the training dataset. Differences between Figure 13 (a) and Figures 14-18 arise, precisely, due to the downsampling.

As for the parameter-tuning process of the GMM models, for each power curve in Figures 14-18, different GMM models with 14 different covariates (cf. Table 1), and varying number of GMM components [cf. Eq. (5)] have been fitted. The parameter tuning of each GMM model has been done using the expectation-maximization algorithm (cf. Section 3).

For the fitted GMM models, their corresponding BIC values are computed so as to select the GMM model that maximizes likelihood and minimizes model-complexity [cf. Eq. (8)]. For each WEF range, the optimal GMM is selected from the tested models, and the selected GMM models represent the expected normal operation of the WPP within the given WEF region.

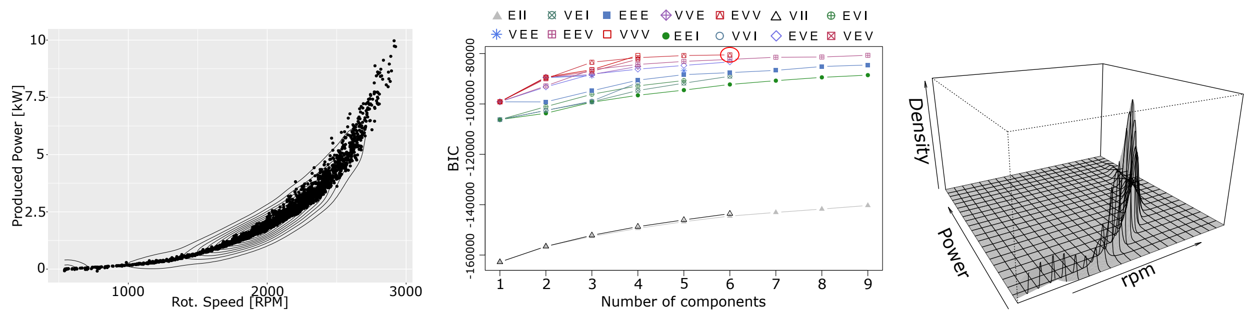

Figure 14: WEF 1: empiric power curve, BIC curves, optimal GMM (6 components, BIC=-80492.11, EVV).

A particularity of the lowest-energetic sea-state WEF 1 in Figure 14 is that the rotational speed never drops below 500 rpm, meaning that the turbine consumes energy from the grid in order to prevent the turbine from stopping. Thus, the turbine is effectively running on idle, which allows for a more efficient restart.

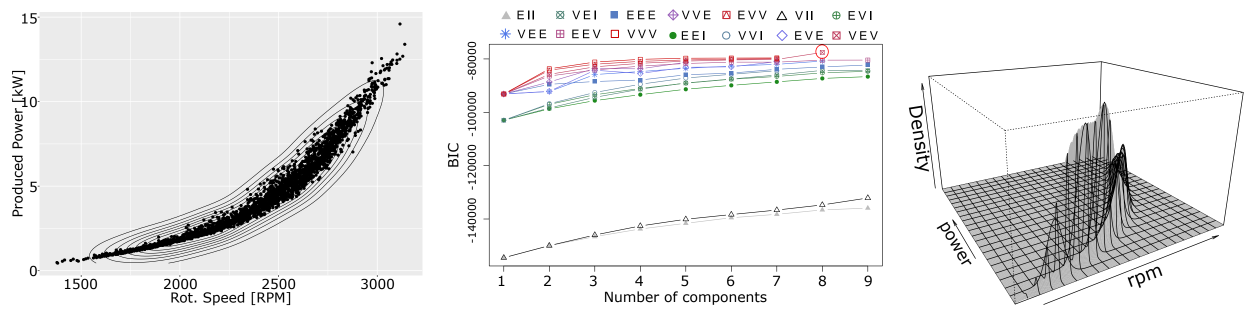

Figure 15: WEF 2: empiric power curve, BIC curves, optimal GMM (8 components, BIC=-77567.86, VEV).

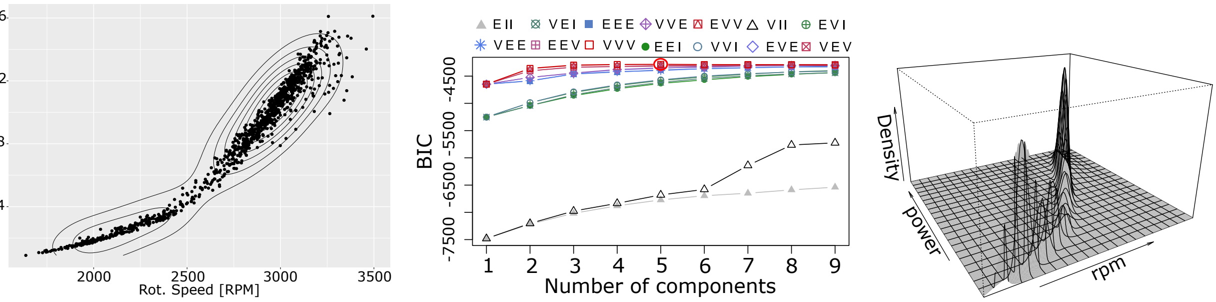

Figure 16: WEF 3: empiric power curve, BIC curves, optimal GMM (5 components, BIC=-42830.23, VVV).

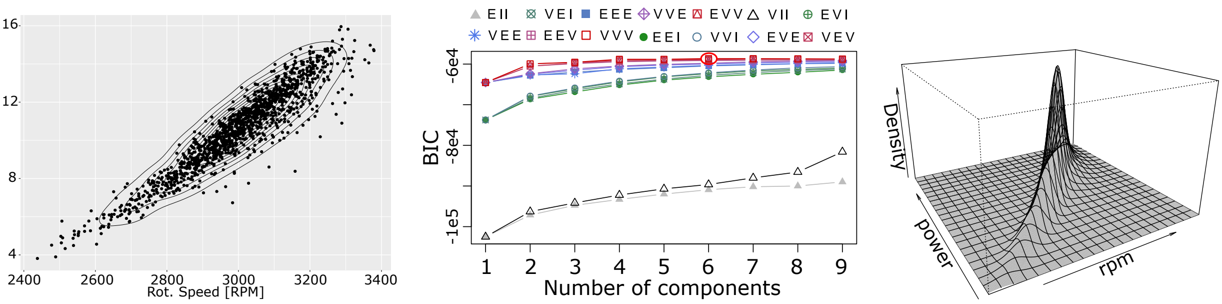

Figure 17: WEF 4: empiric power curve, BIC curves, optimal GMM (6 components, BIC=-58626.75, VVV).

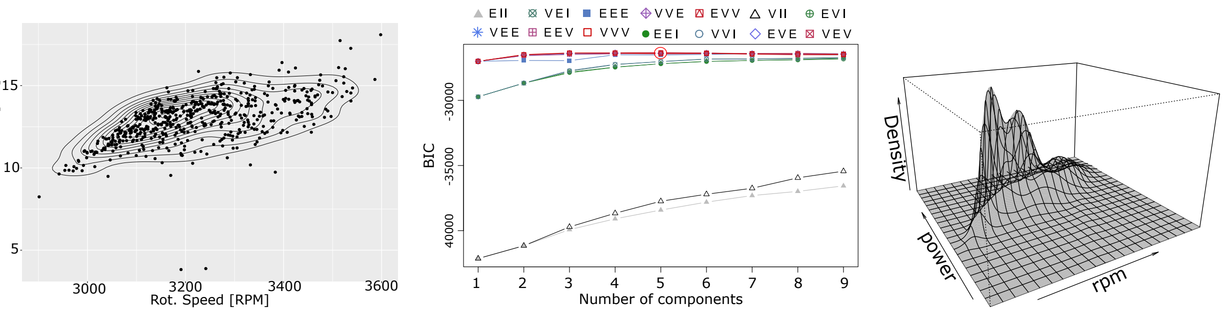

Figure 18: WEF 5: empiric power curve, BIC curves, optimal GMM (5 components, BIC=-26331.96, EVV).

It can be observed from the power curves in Figures 14-18 that the generated power and rotational speed of the different power curves increase from low-energetic sea-states (cf. WEF 1, Figure 14), to high-energetic sea-states (cf. WEF 5, Figure 18). Accordingly, probabilistic regions have been assigned to each WEF region defined by the fitted GMM, which reflects the likely expected operation conditions, given the specific sea-state conditions.

In parallel, for comparison purposes, the empirical power curve and the GMM have been also fitted for the case without division into sea-states. Figure 19 shows the empirical distribution, BIC curves and the optimal GMM model.

From Figure 19, it can be observed that the assigned likelihood values for the value pair power and rotational speed, are different from the likelihood values assigned in Figures 14-18 to the different value pairs of power and rotational speed. As it will be shown, this will have a direct impact on the performance of the conditional anomaly detection model when it

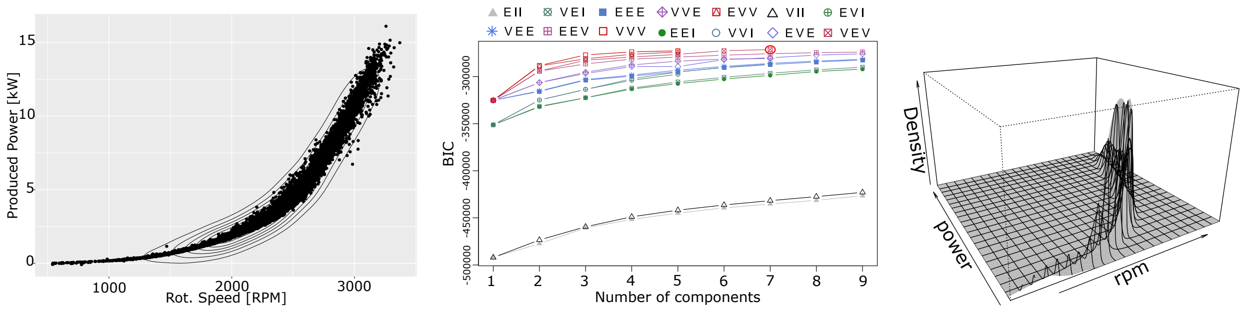

Figure 19: No-States: empiric power curve, BIC curves, optimal GMM (7 components, BIC=-271283.8, VEV).

is informed about different sea-states, and when it ignores the information of different sea states.

Subsequently, after learning the GMM models, for testing purposes, depending on the observed sea-state condition, the corresponding anomaly detection model is activated to detect anomalies. In this way, each independent anomaly detection model focuses on identifying deviations from expected operation conditions for the considered WEF group. The main implementation steps of the anomaly detection process are defined as follows:

1. Read pair $\langle H_s, T_p \rangle$
2. Calculate WEF and identify sea-state group
3. Estimate likelihood of the reading via GMM of the corresponding WEF
4. Evaluate log-likelihood value and determine anomaly

Figure 20 shows anomaly detection results for the different energetic sea-states along with the model without classification into sea-states. The vertical axis has been transformed into log-likelihood scale for anomaly representation purposes Song et al. (2007). The lower the log-likelihood, the more likely to be an anomalous event, because it represents an unlikely situation. Three different threshold levels have been represented so as to show the effect of different boundaries on triggering anomalous events: (a) -12.5, (b) -25 and (c) -50 in the log-scale.

From Figure 20 it can be observed that there is a variation in the sea states across the analysed period along with the obtained log-likelihood values. It can be also seen the inferred log-likelihood value differences between the classification into different sea-states (WEF 1-5) and no-classification of sea-states (no states). This is expected from the fitted GMM models for WEF 1-5 (Figures 14-18) and the GMM with no-states (Figure 19).

As for the different failure threshold levels, for example, for the threshold level (c), the no-states configuration identifies three anomalies, while the state-based anomaly detection matches only with one of them corresponding to the sea-state WEF 2. The subsequent analysis will elaborate further the results shown in Figure 20 focusing on the analysis of the events (#1)-(#2) and (#3)-(#4) that correspond, respectively, to the sea states WEF 5 and WEF 2.

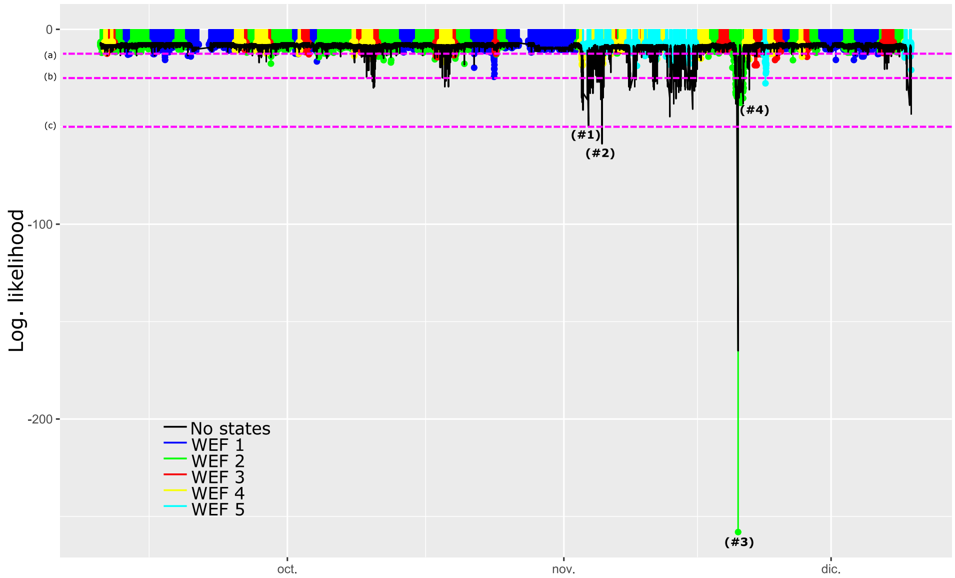

Figure 20: Anomaly detection results.

5.4.1. *WEF 2 events*

Figure 21 shows anomaly detection results for sea-state 2 (WEF 2) along with the corresponding log-likelihood.

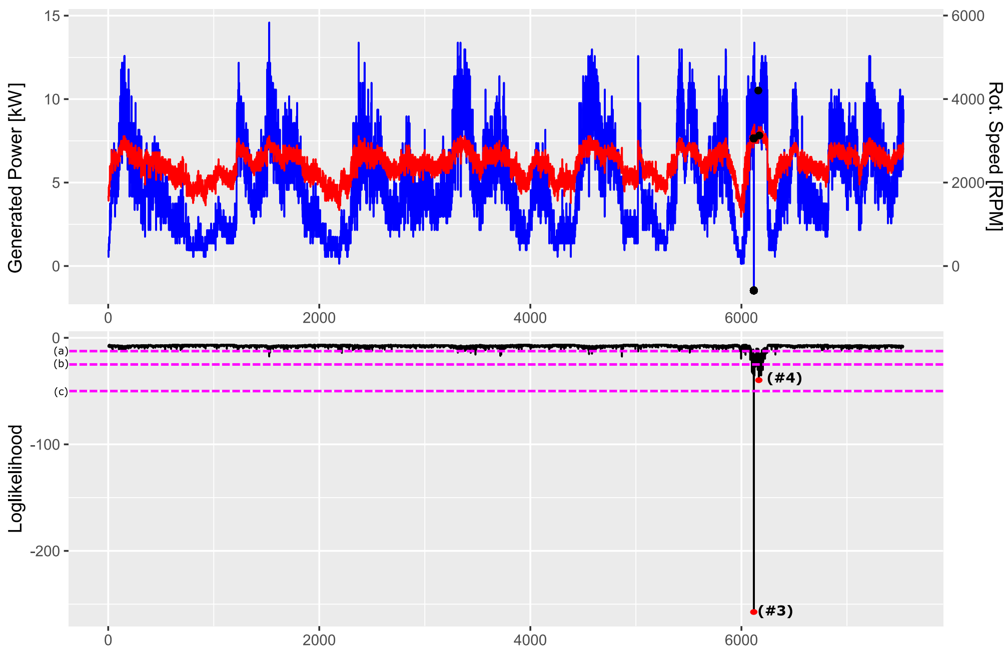

Figure 21: Anomaly detection results for WEF 2.

Figure 21 highlights the potential anomalous events with the corresponding log-likelihood. The lower the likelihood, the lower the occurrence probability. Focusing on two events with the lowest occurrence likelihood, highlighted with markers in Figure 21, it can be observed that one is below the most restrictive threshold (c), *i.e.* event (#3), and the other is below the threshold (b), *i.e.* event (#4).

Figure 22 shows the expanded time-series of the generated power and rotational speed, corresponding to the anomalous events.

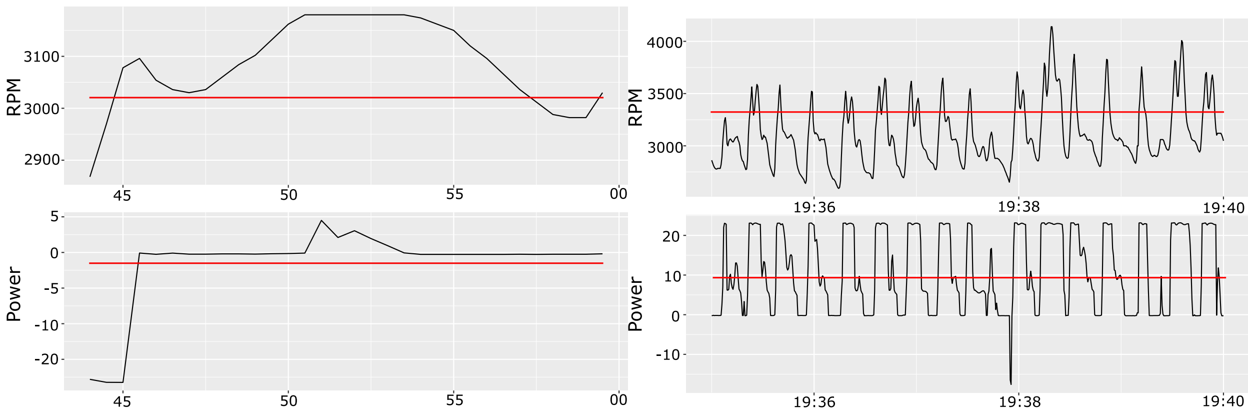

Figure 22: (a) Event (#3) located at 2019-11-20, 13:30; (b) Event (#4) located at 2019-11-20, 19:40.

From Figure 22(a), it can be observed that the averaged power and rotational speed values of the event (#3) are -1.46 kW and 3058.3 rpm, respectively. Comparing these values with the learned GMM of the WEF 2 in Figure 15, it can be inferred that the occurrence likelihood is zero. It can be also noticed in Figure 22(a) that there are only 16 second samples out of the 5-minutes interval, *i.e.* the rest of samples in this interval are zero. This is not flagged as an anomalous plant operation, but an incorrect sensor reading, as confirmed by plant operation experts.

Figure 22(b) shows the corresponding expanded 5-minutes time-series for the event (#4). It can be observed that the averaged power and rotational speed values are 9.77 kW and 3335.09 rpm. Comparing these values with the learned GMM of the WEF 2 in Figure 15, it can be inferred that the occurrence likelihood is not as low as in the previous case, but corresponds to an unlikely event. This is due to the decrease in produced power (see the expected power in Figure 15). This is not a real anomaly and therefore threshold (c) would classify it correctly, while threshold (a) and (b) would missclassify it.

Figure 23 shows the anomaly detection results for the model that does not consider separation of sea-states.

Focusing on the three events below the lowest threshold in Figure 23, it can be observed that the lowest likelihood event (#3) matches with the anomaly flagged by the WEF 2 sea-state GMM model located at 2019-11-20 at 13:30 (cf. Figure 21). As for the event (#4), it can be observed that according to the threshold (c) it would classify it correctly and thresholds (a) and (b) would misclassify the event.

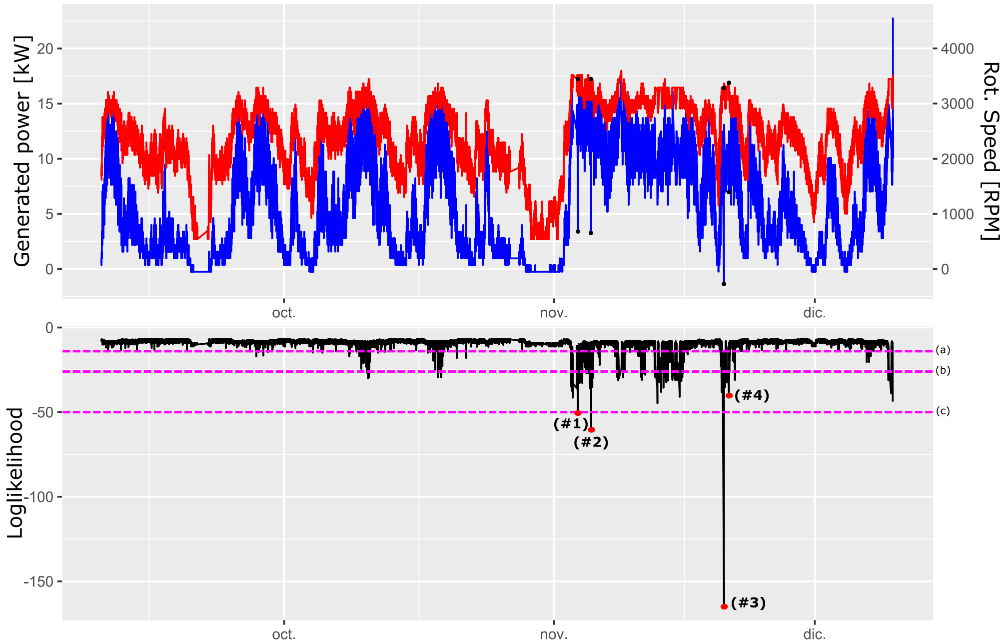

Figure 23: Anomaly detection results without separation into WEF states.

5.4.2. WEF 5 events

There are two additional events associated with the WEF 5 sea-state around first two weeks of November (cf. Figure 25) flagged as anomalies by the model without separation into WEF states. Focusing on the event (#1) located at 2019-11-03 at 18:35 Figure 24(a) shows the expanded 5-minutes time series for power and rotational speed.

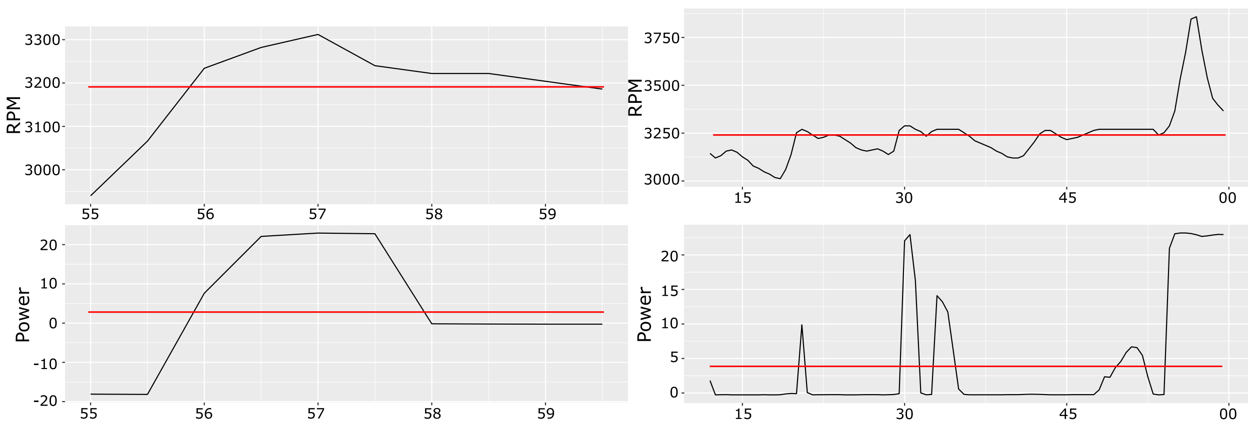

Figure 24: (a) Event (#1) located at 2019-11-03, 18:35; (b) Event (#2) located at 2019-11-05, 06:50.

The mean values for power and rotational speed in Figure 24(a) are 3.82 kW and 3190.8 rpm, respectively. Looking at the GMM of the model without states in Figure 19, it can be observed that the likelihood of this event is low, and this is why the model without states classifies it is as an anomaly. The duration of the event is of 5 seconds out of the 5-minutes interval, which again means that the remainder of readings are zero.

In contrast, focusing on the model inferred from WEF 5 sea-state (cf. Figure 18) it can be seen that there is room for low energy generation. Figure 25 shows individual WEF 5 anomaly detection results.

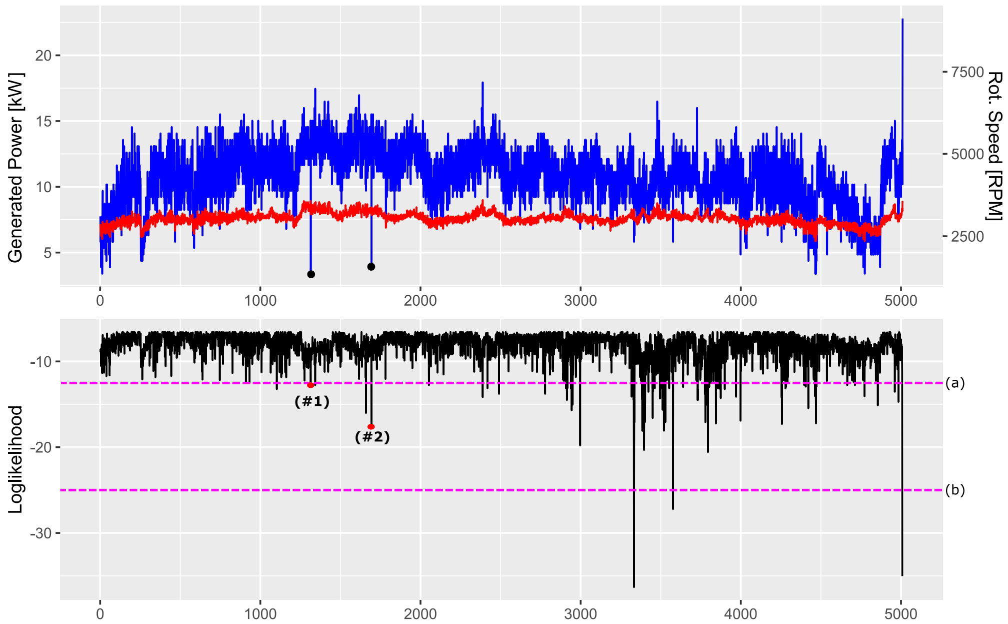

Figure 25: Anomaly detection results for WEF 5.

Therefore, event (#1) is flagged as a false positive event by the model without states, and it is classified correctly for the GMM of the WEF 5, except for the threshold (a).

Focusing on the event (#2) located at 2019-11-05 at 06:50 (cf. Figure 23), Figure 24(b) shows the expanded 5-minutes time series for power and rotational speed. The mean values for power and rotational speed are 4.11 kW and 3241.37 rpm, respectively. The duration of the event is of 1 minute, out of 5 minutes.

Again, analysing the GMM of the model without states in Figure 19, it can be observed that the likelihood of this point is low, and this is why it is regarded as an anomaly by the model without states. In contrast, focusing on the model inferred from WEF 5 sea-state (Figure 18), it can be seen that there is room for low energy generation assigning a higher likelihood compared with the model without states (but still small).

Therefore, event #2, classified as an anomaly by the model without states, is a false positive event and this is captured correctly with the model with states, except for the most restrictive threshold (a).

Table 2 displays the obtained results for the different anomaly detection models including models with and without WEF states and the analysed threshold levels. Additionally, it also shows the performance statistics of the different anomaly detection models.

It can be observed that for the threshold (c) the proposed state-based anomaly detection model obtains the best performance. For the same threshold, the model without states generates false positive events that affect the accuracy of the classifier. For the threshold

Table 2: Summary of anomaly detection results and performance statistics.

Events	Threshold					
	(c)		(b)		(a)	
	States	No-states	States	No-states	States	No-states
Event #1	TN	FP	TN	FP	FP	FP
Event #2	TN	FP	TN	FP	FP	FP
Event #3	TP	TP	TP	TP	TP	TP
Event #4	TN	TN	FP	FP	FP	FP
Accuracy	100%	50%	75%	25%	25%	25%
TNR	100%	33,3%	66,6%	0%	0%	0%
TPR	100%	100%	100%	100%	100%	100%
FPR	0%	50%	25%	75%	75%	75%

[1] **Legend**: True Positive (TP), True Negative (TN), False Positive (FP), False Negative (FN)
[2] $TPR = \frac{TP}{TP+FN}$; $TNR = \frac{TN}{TN+FP}$; $FPR = \frac{FP}{TN+FP}$; $Accuracy = \frac{TP+TN}{TP+TN+FP+FN}$

level (b), the performance of both models decreases and for the most restrictive threshold (a) both models generate false positive events due to the adopted threshold level.

This lead us to draw two main conclusions. The separation of sea-states enables the rational discrimination of expected characteristic power curves given the corresponding sea-states. In contrast, if the whole dataset is considered without considering sea-states, the learned probabilistic distributions are WEF-agnostic and they are prone to misclassifying WPP states as erroneous due to the lack of sea-state information.

6. Discussion

Although the promising results are shown in this paper, before drawing definitive conclusions further work is necessary, contrasting the methodology for other time-periods and turbines. The identification of the most problematic sea-states requires a verified methodology and a significantly larger dataset (a few years of operation) that covers different resource conditions and operation modes. In order to transit towards a scenario where this identification will be possible, some future lines for the improvement of the present approach are suggested here.

Threshold definition without expert knowledge is a challenging task. In some cases, a physical magnitude can be turned into a threshold value. If that is not the case, it may occur that it can be determined by evaluating the probability of occurrence of events. In this research, the effect of different thresholds on different anomalies has been analysed showing that it plays an important role in decision-making. It is possible to extend this work by inferring dynamic thresholds from an statistical analysis, such as Bayesian and Neyman-Pearson hypothesis testing. This will be addressed in future research.

The analysed signals in this work have been post-processed by downsampling them to five minutes average signals. That is, the duration of each point event in the case study is of five minutes. Therefore, if an anomalous event persists for this period, it is considered a non-intermittent event. This was a trade-off decision between complexity and duration of the events. It may have been possible to evaluate the effect of different sampling rates on the anomaly detection approach.

In this research, the identification of sea-states is based on expert knowledge because it is hypothesized that it would be beneficial for the classification of sea-states. The limits between energetic sea-states are deterministic, and therefore, there is room for converting this classification into a data-driven probabilistic approach. Future work will consider the use of trivariate statistical models and copula concepts Jiang et al. (2021) to evaluate data-driven sea-states modelling concepts and compare with expert-based categorization of sea-states.

7. Conclusions

This paper presents a context-informed unsupervised conditional anomaly detection approach for air turbines operated in wave power plants (WPP). The approach has been tested and evaluated in the Mutriku WPP. The proposed approach has been focused on the use of power curves and energetic sea-states formalized through an ensemble of Gaussian Mixture models and expert knowledge.

Results obtained from the application to the Mutriku WPP show the potential of the proposed approach to detect air turbine anomalies through explicit consideration of different sea-states along with power curves. It has been shown that without consideration of sea-state information the anomaly detection model is prone to flag false positive events and the integration of sea-state information aids in the discrimination of anomaly events.

This is part of an ongoing research and authors' plan to extend the anomaly detection approach in different directions including the data-driven inference of anomaly detection thresholds and data-driven identification of sea-states.

Future activities within the prognostics an health management (PHM) framework will focus on the development of diagnostics and prognostics approaches for the WPP components.

Acknowledgment

The authors gratefully acknowledge the Basque Energy Agency (EVE) for supplying the Mutriku wave power plant data and to the Spanish agency Puertos del Estado for providing the metocean data from the SIMAR model and the Bilbao-Vizcaya measuring buoy. J. I. Aizpurua is funded by Juan de la Cierva Incorporacion Fellowship (Spanish State Research Agency - grant number IJC2019-039183-I) and partially supported by the Basque Government (ELKARTEK KK-2021-00021).

References

Aizpurua, J. I., & Catterson, V. M. (2015). Towards a methodology for design of prognostic systems. In *Annual Conference of the Prognostics and Health Management Society 2015* (pp. 504–517).

Aizpurua, J. I., McArthur, S. D. J., Stewart, B. G., Lambert, B., Cross, J. G., & Catterson, V. M. (2019). Adaptive power transformer lifetime predictions through machine learning and uncertainty modeling in nuclear power plants. *IEEE Transactions on Industrial Electronics*, *66*, 4726–4737. doi:10.1109/TIE.2018.2860532.

Aizpurua, J. I., Stewart, B. G., McArthur, S. D. J., Jajware, N., Kearns, M., Garro, U., Muxika, E., & Mendicute, M. (2020). A Diagnostics Framework for Underground Power Cables Lifetime Estimation Under Uncertainty. *IEEE Transactions on Power Delivery*, (pp. 1–1). doi:10.1109/TPWRD.2020.3017951.

Ardhuin, F., Stopa, J. E., Chapron, B., Collard, F., Husson, R., Jensen, R. E., Johannessen, J., Mouche, A., Passaro, M., Quartly, G. D., Swail, V., & Young, I. (2019). Observing sea states. *Frontiers in Marine Science*, *6*, 124. doi:10.3389/fmars.2019.00124.

Baraldi, P., Di Maio, F., Turati, P., & Zio, E. (2015). Robust signal reconstruction for condition monitoring of industrial components via a modified auto associative kernel regression method. *Mechanical Systems and Signal Processing*, *60-61*, 29–44. URL: https://www.sciencedirect.com/science/article/pii/S0888327015000175. doi:https://doi.org/10.1016/j.ymssp.2014.09.013.

Brandsæter, A., Vanem, E., & Glad, I. K. (2019). Efficient on-line anomaly detection for ship systems in operation. *Expert Systems with Applications*, *121*, 418–437. doi:https://doi.org/10.1016/j.eswa.2018.12.040.

Catterson, V. M., McArthur, S. D., & Moss, G. (2010). Online conditional anomaly detection in multivariate data for transformer monitoring. *IEEE Transactions on Power Delivery*, *25*, 2556–2564.

Celeux, G., & Govaert, G. (1995). Gaussian parsimonious clustering models. *Pattern Recognition*, *28*, 781–793. doi:https://doi.org/10.1016/0031-3203(94)00125-6.

Coraddu, A., Lim, S., Oneto, L., Pazouki, K., Norman, R., & Murphy, A. J. (2019). A novelty detection approach to diagnosing hull and propeller fouling. *Ocean Engineering*, *176*, 65–73. doi:https://doi.org/10.1016/j.oceaneng.2019.01.054.

Cottura, L., Caradonna, R., Ghigo, A., Novo, R., Bracco, G., & Mattiazzo, G. (2021). Dynamic Modeling of an Offshore Floating Wind Turbine for Application in the Mediterranean Sea. *Energies*, *14*. doi:10.3390/en14010248.

European Commision Communication (2019). *The European Green Deal*. Technical Report COM(2019) 640 European Commision Brussels. URL: https://eur-lex.europa.eu/resource.html?uri=cellar:b828d165-1c22-11ea-8c1f-01aa75e

European Commision Communication (2020). *Stepping up Europe's 2030 climate ambition. Investing in a climate-neutral future for the benefit of our people*. Technical Report COM(2020) 562 European Commision Brussels. URL: https://eur-lex.europa.eu/legal-content/EN/TXT/PDF/?uri=CELEX:52020DC0562&from=EN.

Falcao, A. F. O., & Gato, L. M. C. (2012). Comprehensive Renewable Energy. chapter Air Turbines. (pp. 111–149). Elsevier volume 8.

Fäy, F.-x., Robles, E., Marcos, M., & Aldaiturriaga, E. (2020). Sea trial results of a predictive algorithm at the Mutriku Wave power plant and controllers assessment based on a detailed plant model. *Renewable Energy*, *146*, 1725–1745. doi:10.1016/j.renene.2019.07.129.

Feng, Y., Qiu, Y., Crabtree, C. J., Long, H., & Tavner, P. J. (2013). Monitoring wind turbine gearboxes. *Wind Energy*, *16*, 728–740. doi:https://doi.org/10.1002/we.1521. arXiv:https://onlinelibrary.wiley.com/doi/pdf/10.1002/we.1521.

Fäy, F.-X., Henriques, J. C., Kelly, J., Mueller, M., Abusara, M., Sheng, W., & Marcos, M. (2020). Comparative assessment of control strategies for the biradial turbine in the mutriku owc plant. *Renewable Energy*, *146*, 2766–2784. URL: https://www.sciencedirect.com/science/article/pii/S0960148119312613. doi:https://doi.org/10.1016/j.renene.2019.08.074.

Fäy, F.-X., Kelly, J., Henriques, J., Pujana, A., Abusara, M., Mueller, M., Touzon, I., & Ruiz-Minguela, P. (2018). Numerical Simulation of Control Strategies at Mutriku Wave Power Plant. volume Volume 10: Ocean Renewable Energy of *International Conference on Offshore Mechanics and Arctic Engineering*. URL: https://doi.org/10.1115/OMAE2018-78011. doi:10.1115/OMAE2018-78011. arXiv:https://asmedigitalcollection.asme.org/OMAE/proceedings-pdf/OMAE2018/51319/V0 v010T09A029.

Galloway, G. S., Catterson, V. M., Love, C., Robb, A., & Fay, T. (2017). Modeling and interpretation of tidal turbine vibration through weighted least squares regression. *IEEE Transactions on Systems, Man, and Cybernetics: Systems*, *50*, 1252–1259.

Gilbert, C., Browell, J., & McMillan, D. (2021). Probabilistic access forecasting for improved offshore operations. *International Journal of Forecasting*, *37*, 134–150. doi:https://doi.org/10.1016/j.ijforecast.2020.03.007.

Gill, S., Stephen, B., & Galloway, S. (2012). Wind turbine condition assessment through power curve copula modeling. *IEEE Transactions on Sustainable Energy*, *3*, 94–101. doi:10.1109/TSTE.2011.2167164.

Guanche, R., Martini, M., Jurado, A., & Losada, I. J. (2016). Walk-to-work accessibility assessment for floating offshore wind turbines. *Ocean Engineering*, *116*, 216–225. doi:https://doi.org/10.1016/j.oceaneng.2016.03.013.

Gupta, S. C., & Nem, R. K. (2016). A Critical Review on Wind Turbine Power Curve Modelling Techniques and Their Applications in Wind Based Energy Systems. *Journal of Energy*, .

Hameed, Z., Hong, Y., Cho, Y., Ahn, S., & Song, C. (2009). Condition monitoring and fault detection of wind turbines and related algorithms: A review. *Renewable and Sustainable Energy Reviews*, *13*, 1–39. doi:https://doi.org/10.1016/j.rser.2007.05.008.

Hines, J. W., & Garvey, D. R. (2006). Development and application of fault detectability performance metrics for instrument calibration verification and anomaly detection. *Journal of Pattern Recognition Research*, (pp. 2–15).

IEA (2019). *Offshore Wind Outlook 2019*. Technical Report International Energy Agency.

Ioannou, A., Angus, A., & Brennan, F. (2018). A lifecycle techno-economic model of offshore wind energy for different entry and exit instances. *Applied Energy*, *221*, 406–424. doi:https://doi.org/10.1016/j.apenergy.2018.03.143.

Islam, M. S., Khreich, W., & Hamou-Lhadj, A. (2018). Anomaly detection techniques based on kappa-pruned ensembles. *IEEE Transactions on Reliability*, *67*, 212–229. doi:10.1109/TR.2017.2787138.

Jiang, H., Bai, X., Song, G., Luo, M., & Ma, X. (2021). Comparing trivariate models for coastal winds and waves accounting for monthly seasonality. *Applied Ocean Research*, *117*, 102959. doi:https://doi.org/10.1016/j.apor.2021.102959.

Jlassi, I., Estima, J. O., Khojet El Khil, S., Mrabet Bellaaj, N., & Marques Cardoso, A. J. (2015). Multiple open-circuit faults diagnosis in back-to-back converters of pmsg drives for wind turbine systems. *IEEE Transactions on Power Electronics*, *30*, 2689–2702. doi:10.1109/TPEL.2014.2342506.

Kusiak, A., Zhang, Z., & Verma, A. (2013). Prediction, operations, and condition monitoring in wind energy. *Energy*, *60*, 1–12. doi:https://doi.org/10.1016/j.energy.2013.07.051.

Lekube, J., Ajuria, O., Ibeas, M., Igareta, I., & Gonzalez, A. (2018). Fatigue and aerodynamic loss in wells turbines : Mutriku wave power plant case. In *International Conference on Ocean Energy, Cherbourg, France*.

Lekube, J., Garrido, A. J., & Garrido, I. (2016). Rotational speed optimization in oscillating water column wave power plants based on maximum power point tracking. *IEEE Transactions on Automation science and Engineering*, *14*, 681–691.

Martinez, A., & Iglesias, G. (2022). Mapping of the levelised cost of energy for floating offshore wind in the european atlantic. *Renewable and Sustainable Energy Reviews*, *154*, 111889. doi:https://doi.org/10.1016/j.rser.2021.111889.

Martinez-Luengo, M., Kolios, A., & Wang, L. (2016). Structural health monitoring of offshore wind turbines: A review through the statistical pattern recognition paradigm. *Renewable and Sustainable Energy Reviews*, *64*, 91–105. doi:https://doi.org/10.1016/j.rser.2016.05.085.

Martinez-perurena, A., Penalba, M., & Aizpurua, J.-I. (2021). Machine-Learning-based Long-Term Forecasting of Metocean Data for the Design of Marine Renewable Energy Systems. In *Sustainable Development of Energy, Water and Environment Systems (SDEWES)* 545. Dubrovnik, Croatia.

Mérigaud, A., & Ringwood, J. V. (2016). Condition-based maintenance methods for marine renewable energy. *Renewable and Sustainable Energy Reviews*, *66*, 53–78.

Michau, G., & Fink, O. (2021). Unsupervised transfer learning for anomaly detection: Application to complementary operating condition transfer. *Knowledge-Based Systems*, *216*, 106816. URL: https://www.sciencedirect.com/science/article/pii/S0950705121000794. doi:https://doi.org/10.1016/j.knosys.2021.106816.

Mørk, G., Barstow, S., Kabuth, A., & Pontes, M. T. (2010). Assessing the Global Wave Energy Potential. (pp. 447–454). volume 29th International Conference on Ocean, Offshore and Arctic Engineering: Volume 3 of *International Conference on Offshore Mechanics and Arctic Engineering*. doi:10.1115/OMAE2010-20473.

Mérigaud, A., & Ringwood, J. V. (2018). Free-surface time-series generation for wave energy applications. *IEEE Journal of Oceanic Engineering*, *43*, 19–35. doi:10.1109/JOE.2017.2691199.

de Novaes Pires Leite, G., Araújo, A. M., & Rosas, P. A. C. (2018). Prognostic techniques applied to maintenance of wind turbines: a concise and specific review. *Renewable and Sustainable Energy Reviews*, *81*, 1917–1925. doi:https://doi.org/10.1016/j.rser.2017.06.002.

Otaola, E., Garrido, A. J., Lekube, J., & Garrido, I. (2019). A comparative analysis of self-rectifying turbines for the mutriku oscillating water column energy plant. *Complexity*, *2019*.

Pandit, R. K., & Infield, D. (2018). Scada-based wind turbine anomaly detection using gaussian process models for wind turbine condition monitoring purposes. *IET Renewable Power Generation*, *12*, 1249–1255.

Penalba, M., & Ringwood, J. (2016). A review of wave-to-wire models for wave energy converters. *Energies*, *9*. doi:10.3390/en9070506.

Reguero, B. G., Losada, I. J., & Méndez, F. J. (2015). A global wave power resource and its seasonal, interannual and long-term variability. *Applied Energy*, *148*, 366 – 380. doi:http://dx.doi.org/10.1016/j.apenergy.2015.03.114.

Rinaldi, G., Garcia-Teruel, A., Jeffrey, H., Thies, P. R., & Johanning, L. (2021a). Incorporating stochastic O&M models into the techno-economic analysis of floating offshore wind farms. *Applied Energy*, *301*, 117420. doi:10.1016/j.apenergy.2021.117420.

Rinaldi, G., Thies, P. R., & Johanning, L. (2021b). Current status and future trends in the operation and maintenance of offshore wind turbines: A review. *Energies*, *14*. doi:10.3390/en14092484.

Ruggiero, P., Komar, P. D., & Allan, J. C. (2010). Increasing wave heights and extreme value projections: The wave climate of the u.s. pacific northwest. *Coastal Engineering*, *57*, 539–552. URL: https://www.sciencedirect.com/science/article/pii/S0378383909002142. doi:https://doi.org/10.1016/j.coastaleng.2009.12.005.

Santos, F., Teixeira, A. P., & Guedes-Soares, C. (2015). Modelling and simulation of the operation and maintenance of offshore wind turbines. *Proceedings of the Institution of Mechanical Engineers, Part O: Journal of Risk and Reliability*, *229*, 385–393. doi:10.1177/1748006X15589209.

Scrucca, L., Fop, M., Murphy, T. B., & Raftery, A. E. (2016). mclust 5: clustering, classification and density estimation using Gaussian finite mixture models. *The R Journal*, *8*, 289–317.

Song, X., Wu, M., Jermaine, C., & Ranka, S. (2007). Conditional anomaly detection. *IEEE Transactions on Knowledge and Data Engineering*, *19*, 631–645. doi:10.1109/TKDE.2007.1009.

Sorensen, J. D., & Sorensen, J. N. (2012). *Wind energy systems: Optimising design and construction for safe and reliable operation*. Woodhead Publishing, Ltd.

Torre-Enciso, Y., Ortubia, I., De Aguileta, L. L., & Marqués, J. (2009). Mutriku wave power plant: from the thinking out to the reality. In *Proceedings of the 8th European wave and tidal energy conference, Uppsala, Sweden* (pp. 319–329). volume 710.

Tucker, M., & Pitt, E. (2001). *Waves in Ocean Engineering*. Elsevier Ocean Engineering Series. Elsevier Science.

Ulazia, A., Esnaola, G., Serras, P., & Penalba, M. (2020). On the impact of long-term wave trends on the geometry optimisation of oscillating water column wave energy converters. *Energy*, *206*, 118146. URL: https://linkinghub.elsevier.com/retrieve/pii/S0360544220312536. doi:10.1016/j.energy.2020.118146.

Ulazia, A., Penalba, M., Ibarra-Berastegui, G., Ringwood, J., & Saénz, J. (2017). Wave energy trends over the bay of biscay and the consequences for wave energy converters. *Energy*, *141*, 624–634. doi:https://doi.org/10.1016/j.energy.2017.09.099.

Vachtsevanos, G., Lewis, F., Roemer, M., Hess, A., & Wu, B. (2006). *Intelligent Fault Diagnosis and Prognosis for Engineering Systems*. John Wiley & Sons, Ltd. doi:https://doi.org/10.1002/9780470117842.

Vanem, E., & Brandsæter, A. (2021). Unsupervised anomaly detection based on clustering methods and sensor data on a marine diesel engine. *Journal of Marine Engineering & Technology*, *20*, 217–234. doi:10.1080/20464177.2019.1633223.

Vedreño-Santos, F., Riera-Guasp, M., Henao, H., Pineda-Sánchez, M., & Puche-Panadero, R. (2014). Diagnosis of Rotor and Stator Asymmetries in Wound-Rotor Induction Machines Under Nonstationary Operation Through the Instantaneous Frequency. *IEEE Transactions on Industrial Electronics*, *61*, 4947–4959. doi:10.1109/TIE.2013.2288192.

Walsh, J., Bashir, I., Garrett, J. K., Thies, P. R., Blondel, P., & Johanning, L. (2017). Monitoring the condition of marine renewable energy devices through underwater acoustic emissions: Case study of a wave energy converter in falmouth bay, uk. *Renewable Energy*, *102*, 205–213. doi:https://doi.org/10.1016/j.renene.2016.10.049.

Wu, J., Zhao, Z., Sun, C., Yan, R., & Chen, X. (2020). Fault-attention generative probabilistic adversarial autoencoder for machine anomaly detection. *IEEE Transactions on Industrial Informatics*, *16*, 7479–7488. doi:10.1109/TII.2020.2976752.

Yue, C.-D., Liu, C.-C., Tu, C.-C., & Lin, T.-H. (2019). Prediction of Power Generation by Offshore Wind Farms Using Multiple Data Sources. *Energies*, *12*. doi:10.3390/en12040700.